High-performance wafer-scale transfer-free graphene microphones

Pezone, Roberto; Baglioni, G.; Sarro, Pasqualina M.; Steeneken, Peter G.; Vollebregt, Sten

DOI
10.1109/MEMS49605.2023.10052360

Publication date
2023

Document Version
Final published version

Published in
Proceedings of the 2023 IEEE 36th International Conference on Micro Electro Mechanical Systems (MEMS)

HIGH-PERFORMANCE WAFER-SCALE TRANSFER-FREE GRAPHENE MICROPHONES

Roberto Pezone[1], Gabriele Baglioni[2], Pasqualina M. Sarro[1], Peter G. Steeneken[2,3], and Sten Vollebregt[1]

[1]Laboratory of Electronic Components, Technology and Materials (ECTM), Department of Microelectronics, Delft University of Technology, The Netherlands

[2]Kavli Institute of Nanoscience, Department of Quantum Nanoscience, Delft University of Technology, The Netherlands

[3]Department of Precision and Microsystems Engineering (PME), Delft University of Technology, The Netherlands

2023 IEEE 36th International Conference on Micro Electro Mechanical Systems (MEMS) | 978-1-6654-9308-6/23/$31.00 ©2023 IEEE | DOI: 10.1109/MEMS49605.2023.10052360

ABSTRACT

A repeatable method to fabricate multi-layer graphene (ML-gr) membranes of $2r$ = 85 – 155 μm (t < 10 nm) with a 100% yield on 100 mm wafers is demonstrated. These membranes show higher sensitivity than a commercial MEMS-Mic combined with an area reduction of 10x. The process overcomes one of the main limitations when integrating graphene diaphragms in microphones due to the absence of automatic transfer methods on non-planarized target substrates. This method aims to overcome this limitation by combining a full-dry release of Chemical Vapor Deposition (CVD) graphene by Deep Reactive Ion Etching (DRIE) and vapor HF (VHF).

KEYWORDS

Graphene, Microphone, Membrane, Wafer-Scale, MEMS, Transfer-Free.

INTRODUCTION

Condenser MEMS-Mic lack a clear direction for miniaturization and high performance due to the Si-metal diaphragm's physical properties, i.e., high-tension. The microphone sensitivity S (eq.1) is determined by the membrane displacement per pressure load (C_m) towards the counter electrode at distance x_0 and the constant bias voltage (V_b) that maintains a fixed charge on the electrodes [1].

$$S = \frac{V_b\, C_m}{x_0} \tag{1}$$

To achieve a more significant sensitivity without incurring high power consumption, due to large voltage bias, or microfabrication issues, such as membrane stiction caused by tiny gaps, a higher mechanical compliance (C_m) is needed. Because C_m is inversely proportional to the membrane tension and thickness, graphene, due to its high aspect-ratio, low-tension, and capacity to conduct electrical current, is the perfect candidate for enabling larger deflection under sound pressure for a smaller membrane size. In the last five years, advanced methods to fabricate such large membranes made by CVD graphene, primarily via polymer-based transfer, have been investigated [2 - 10]. However, despite the very high aspect ratios and high crystallinity of the demonstrated free-standing membranes (single-layer and few-layer graphene) in the mentioned works do not provide a clear route toward industrialization of the devices. This is because the transfer-based methods employed are not easily scalable toward high-volume wafer-level fabrication. The main reason is addressed to the absence of commercial equipment for transferring graphene over large cavities. Furthermore, current transfer methods often suffer from low yield, polymer contamination, cracks, and folding, leading to adhesion issues, especially for non-planarized target substrates. This work proposes an alternative approach in order to overcome these limitations with a wafer-scale transfer-less method where multi-layered graphene (ML-gr) drums are grown and released on the same substrate. More than 50 membranes with $2r$ = 85 – 300 μm have been measured, showing a great tension uniformity. Peak mechanical compliances of ≈ 92 nm Pa^{-1} and ≈ 9 nm Pa^{-1} for the proposed membranes of $2r$ = 300 μm and $2r$ = 85 – 155 μm are obtained. A 100% yield of functional devices with diameters between $2r$ = 85 – 155 μm is shown, differently than the 18% yield of the $2r$ = 300 μm membranes.

EXPERIMENTAL SECTION

Process-flow

A 100 mm Si p-type wafer is thermally oxidized, forming 1 μm of SiO_2. LPCVD silicon-rich low-stress silicon nitride (110 nm, SiH_2Cl_2 315 sccm/NH_3 85 sccm) at 850 °C is first deposited and then patterned on the top-side and entirely removed on the back-side. PECVD TEOS-based 5 μm-thick silicon oxide is deposited on the back-side to be used as an etching mask for the bulk Si DRIE. A thin film of 50 nm molybdenum is sputtered at 50°C and etched by dry-etching with Cl and O_2 chemistry. The photoresist is stripped by O_2 plasma followed by rinsing in N-methyl-2-pyrrolidone (NMP) and DI-water (Fig. 1 (1)). Graphene is synthesized at 935 °C with an AIXTRON Black Magic at 25 mbar and H_2/CH_4 gas sources (Fig. 1 (2)). Next, Cr/Au (20/200 nm) is evaporated by ion-beam evaporation and patterned using a lift-off technique with NMP at 65 °C (Fig. 1 (3)). Mo is wet-etched with H_2O_2 and rinsed with DI-water (Fig. 1 (4)). The Bosch process is used to etch the bulk Si on the back-side with the graphene side facing the chuck, avoiding SF_6 exposure (Fig. 1 (5)). Finally, VHF etch is performed at 45 °C with 100% anhydrous HF, N_2, and EtOH in a commercially available Primaxx μEtch system, at 125 Torr, on diced chips of 10 mm x 10 mm (Fig. 1 (6)). All the residuals originating from the LPCVD SiN_x and VHF reaction are removed with a post-bake at T > 110 °C in vacuum.

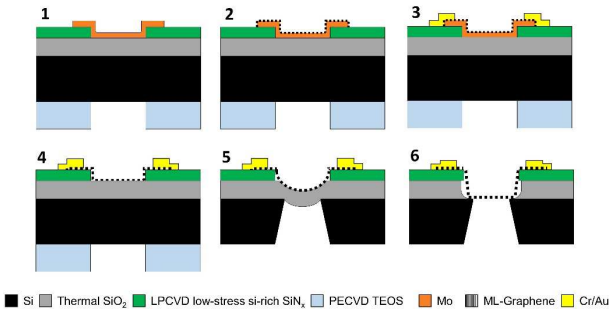

Figure 1: Main fabrication steps. (1) Patterning of the 110 nm SiN_x layer (top-side) and 5 µm PECVD TEOS layer (back-side). Sputtering and dry-etching of 50 nm Mo. (2) Graphene CVD at 935 °C and 25 mbar. (3) Cr/Au (20/200 nm) evaporation and patterning by lift-off, which are used as additional anchoring and electrical contact. (4) Mo wet-etching in H_2O_2. (5) Backside DRIE of bulk Si. (6) Vapor HF of thermal SiO_2 (950 nm).

Acoustic measurement setup

A reference microphone (Sonarworks XREF20) measures the input sound pressure from the speaker, and it is placed close to the sample to have equidistance from the loudspeaker, avoiding significant phase differences. The signal captured by the reference microphone, the mechanical frequency response of the graphene membrane detected by the Polytec vibrometer at the center of the membrane, and the output signal of the speaker are monitored by a Moku:Lab (Liquid Instruments) hardware platform. The mechanical compliance is obtained from the ratio of the two signals received by the Moku:Lab after correction and calibration steps of the corresponding sensitivities of the vibrometer controller and reference microphone. Acoustic actuation at a sound pressure level of 1 Pa (≈ 94 dB SPL) is used to test the fabricated membranes [11].

RESULTS AND DISCUSSION

Membrane fabrication

The fabricated heterostructures composed of SiO_2/ML-gr (before VHF) and the released ML-gr (after VHF) show different topography under optical inspection by a 3D laser scanning confocal microscope. A maximum downward out-of-plane deflection ranging from $h_0 = 3.05 – 6.08$ µm for membranes with $2r = 85 – 155$ µm and $10 – 11.4$ µm for $2r = 300 – 350$ µm are measured. A buckling state addresses these deformations due to different thermal expansion coefficients between the SiO_2 layer and Si substrate. After the VHF release of the SiO_2 layer, the ML-gr recovers its original flat shape in the suspended region, showing nano-wrinkling due to imprinting left by the Mo topography on which graphene was grown (Fig. 2b). In addition, after the release, due to the thin SiO_2 film, the graphene attaches to the Si substrate, probably because of sagging or stiction during the final release. With a laser 3D microscope, a step height of ≈ 1.3 µm, equal to the sum of the thickness of the SiO_2, SiN_x, and the electrode, is measured, confirming its collapse on the silicon underneath (Fig. 2b). All Membranes with diameters of $2r = 85 – 155$ µm show a 100% yield with all 132 suspended devices surviving after the vapor HF

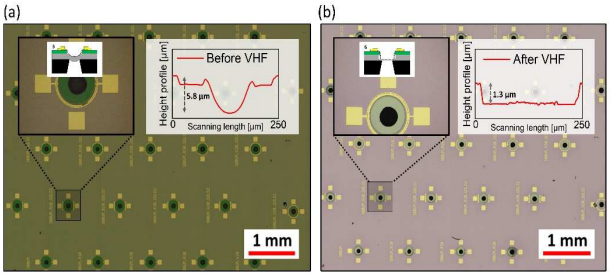

Figure 2: Chip-view with topographic analysis along each membrane before and after SiO_2 etching by using 3D laser scanning confocal microscope. (a) Suspended SiO_2/ML-gr heterostructure with step height measurement of one single drum showing 1st mode buckling deformation. (b) Released ML-gr (after VHF) where buckling has disappeared showing a flat suspended membrane. These results are extendable to all devices present in the chips with only some small peak height variations due to membrane size differences.

release. Large SiO_2/ML-gr heterostructures with diameters of 300–350 µm show a 37% yield on 117 fabricated drums after the DRIE. After SiO_2 etching, the same drums decrease their yield from 37% to 18%. Larger membranes have lower yield because of higher buckling modes that cause significant distortions, cracks, and high deformations in the oxide, compared to the first modes that have been found for 2r = 85–155 µm membranes. This can be improved by tuning the stress of the SiO_2 film or compensating the compressive stress with the tensile SiN_x frames [12].

Graphene characterization

A Horiba HR800 Raman spectrometer equipped with a 514.5 nm Ar^+ laser maintained at 5mW is used to inspect the crystallinity of the 25 test drums before and after the VHF step. A 100× objective with a numerical aperture of 0.9 is used with a spot size of about 696 nm. A large defectivity is highlighted for the final ML-gr drums, with I_D/I_G ranging from 0.52 – 0.88 after normalization with respect to the G-band of the measured data. The high D band is related to any kind of defect that distorts the graphene lattice, like edges, wrinkles, Stone–Wales defects, and vacancies. In addition, the D intensity shows the invasiveness of the process on the graphene compared to previous works where lower defect intensity was reported for the same material [13]. This increased defectivity source could be attributed to the lift-off step where NMP or the short ultrasonic bath has probably negatively affected the quality of the material. Finally, it can be seen that the Raman 2D-peak ratios are representative of multi-layer graphene, as shown in Fig. 3a, where $I_{2D}/I_G < 1$ are measured [14]. The difference in I_D/I_G, I_{2D}/I_G is due to thickness variation and variations in the number of defects. A graphene thickness of ≈ 7 ± 2 nm is measured with an atomic force microscope (AFM) from Cypher Asylum Research in semi-contact mode (Fig. 3b). The AFM thickness measurements are made on graphene which is processed with all the reported steps except the VHF. Since the SiN_x cannot be marked as flat reference point due to a partial over-etching during Mo

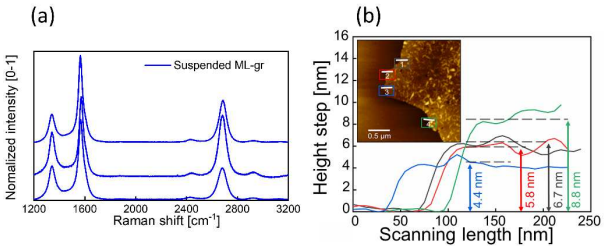

Figure 3: (a) Raman spectrum from 1200 to 3200 cm^{-1} of three different ML-gr drums in the suspended region. The difference in I_D/I_G, I_{2D}/I_G is due to thickness variation and variations in the number of defects.(b) Thickness measurement of the ML-gr after transfer on bare Si/SiO_2 substrate by AFM in semi contact mode.

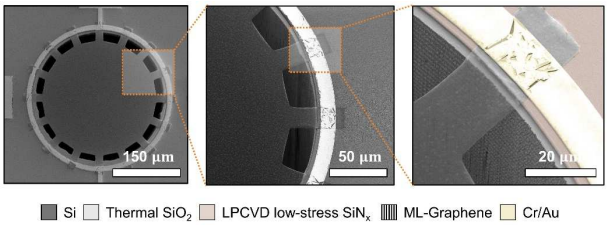

Figure 4: Scanning electron microscope (SEM) pictures made by a Hitachi Regulus 8230 of suspended 300 µm trampoline ML-gr.

patterning, it is transferred in DI-water on a clean thermally oxidized silicon chip. Fig. 4 shows a suspended membrane that is patterned in a trampoline geometry with a diameter of 300 µm where the Cr–Au/SiN_x/Si interface acts as a clamping support for the suspended graphene.

Resonance frequency and mechanical compliance

Dynamic visualization of the proposed membranes is managed by a digital holographic microscope (LynceeTec) equipped with a laser wavelength of 666 nm and a 10x objective lens in stroboscopic mode. The interference between the reflected laser beam from the sample and the reference path provides the intensity and phase of each pixel, defining the 3D topography. At its resonance frequency, mechanical motion is exhibited because of the optical phase shifts that result from the oscillating membrane. Mounting 1 x 1 cm chips on a piezo-shaker controlled by a sine wave with 0.5V and a frequency range f_0 = 50 – 350 kHz in a vacuum chamber at 10^{-4} kPa to reduce any air damping effects, the first mode of the resonance frequencies are visualized. More than ten membranes have been inspected, and they show resonance frequencies over ≈ 244 – 318 kHz for diameters of $2r$ = 120 – 155 µm as shown in Fig. 5a. Using a graphene thickness of 7 nm, a density of 2260 kg/m^3, a diameter range of 120 – 155 µm, the experimental results fit the analytical values in a pre-tension range of n_0 = 0.03 – 0.05 N/m. The analytical values are calculated with Eq. 2 [15],

$$f_0 = \frac{2.405}{2\pi R}\sqrt{\frac{n_0}{\rho t}} \qquad (2)$$

where n_0 is the pre-tension (N/m) of the graphene, ρ the mass density, and t is the thickness of the graphene. Here, the bending rigidity influence is omitted since it is estimated to be small. The membrane displacement z caused by sound actuation is measured by a single-point laser Doppler vibrometer (LDV, OFV-5000 Polytec GmbH) at the drum's center, where the most significant deflection is expected. The obtained results are referred to a sound pressure of 1 Pa (94 dB). More than 50 devices with diameters ranging from 85 – 300 µm are inspected, showing a mechanical compliance range of ≈ 3 – 92 nm Pa^{-1} at 1 kHz as shown in Fig. 5b. This specific frequency is considered to be the middle of the audio band where the human ear has the highest sensitivity. Then, the analytical results are calculated and compared with the experimental ones according to Eq. 3 where the displacement z is quadratically related to the membrane size [15]. More importantly, the cubic terms in z are neglected due to the linear regime in this relation. The proposed drums are compared with the experimental results in Fig. 5b. Within the $2r$ = 85 – 155 µm, the quadratic dependency is found with a pre-tension fit n_0 of 0.2 N/m, unlike the larger membranes with 2r = 300 µm that show n_0 of 0.07 – 0.1 N/m depending on their clamping geometry.

$$\Delta P = \frac{4n_0 z}{R^2} \qquad (3)$$

Spring structures show lower pre-tension of ≈ 0.03 N/m compared the fully-clamped (≈ 0.1 N/m) for same membrane diameter of 300 µm. This also translates in a 1.4 times higher mechanical compliance of the spring structure than the fully-clamped. The quadratic dependency is not shown in the entire diameter range of 85 – 300 µm, and the reason might be addressed to a more profound sagging of larger membranes compare to the smaller one. When comparing the pre-tension extracted from Eq. 2 - 3, we note that different values of n_0 are obtained as in Fig 5a, b. These differences might be caused by uncertainty in the mass and thickness that affect Eq. 2, gas damping and permeation effects at 1 kHz that affect Eq. 3, and differences in the deflected mode shapes from theory.

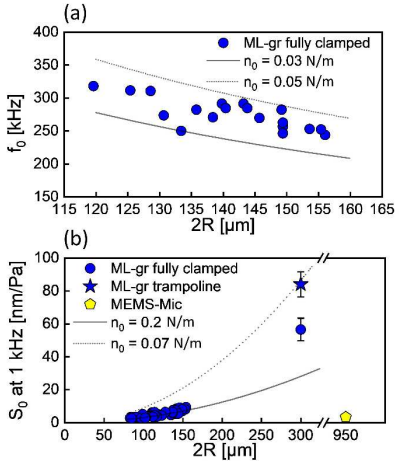

Figure 5: Resonance frequency and mechanical compliance measurements. (a) Resonance frequency for ML-gr with 120–155 um. (b) Comparison of the mechanical compliance of the ML-gr membranes with a commercial MEMS microphone MP23DB01HP, MP34DT04 STMicroelectronics (yellow pentagon).

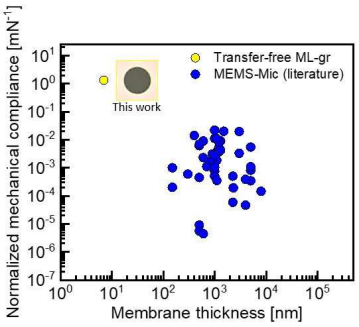

Figure 6: Benchmark of mechanical compliance normalized by the membrane area of proposed ML-gr and MEMS-Si based microphone state-of-the-art.

Additional investigation is needed to quantitatively account for these differences. These compliances exceed that of a larger membrane of 2r = 950 µm used in commercially available MEMS Si microphones. Peak compliance of 92 nm Pa^{-1} is achieved with a *2r* = 300 µm ML-gr trampoline. With this, we demonstrate the potential of graphene for future miniaturized and high-performance microphones as compared to traditional MEMS-Mic (Fig. 6), with a scalable fabrication method suitable for uniform device performance and allowing more accurate, repeatable statistical studies of free-standing graphene-based devices [15].

CONCLUSIONS

This work demonstrates a repeatable and scalable process flow to efficiently fabricate wafer-scale multi-layer graphene drums with diameters from 2*r* = 85 to 300 µm. A 100% yield was demonstrated for membranes with 2r = 85 – 155 µm. These drums can operate as microphones with mechanical compliances up to 92 nm Pa^{-1} that exceeds that of a larger membrane of 2r = 950 µm used in commercially available MEMS Si microphones that generally have few nm Pa^{-1}. The results presented here show the great potential of these devices for next-generation, high-volume, wafer-scale graphene microphone technologies once developed in a capacitive architecture.

ACKNOWLEDGEMENTS

The authors thank the Delft University of Technology Else Kooi Lab staff for processing support and thank Herre van der Zant for useful discussions. This project has received funding from Union's Horizon 2020 research and innovation program under Grant Agreement No. 881603 (Graphene Flagship).

REFERENCES

[1] M. Fueldner, Chapter 48 – Microphones, Handbook of Silicon Based MEMS Materials and Technologies (Third Edition), Elsevier, 2020, pp.937-948.

[2] D. Todorović, A. Matković, M. Milićević, D. Jovanović, R. Gajić, I. Salom and M. Spasenović, "Multilayer Graphene Condenser Microphone", *2D Materials*, 2, 045013, 2015.

[3] S. Woo, J. -H. Han, J. -H Lee, S. Cho, K. -W. Seong, M. Choi, J.-H. Cho, "Realization of a High Sensitivity Microphone for a Hearing Aid Using a Graphene–PMMA Laminated Diaphragm", *ACS Appl. Mater. Interfaces*, 9, 1237– 1246, 2017.

[4] S. Wittmann, C. Glacer, S. Wagner, S. Pindl, M.C. Lemme, "Graphene Membranes for Hall Sensors and Microphones Integrated with CMOS-Compatible Processes", *ACS Applied Nano Materials*, 2, 5079– 5085, 2019.

[5] S. Wagner, C. Weisenstein, A. Smith, M. Östling, S. Kataria, M. Lemme, "Graphene Transfer Methods for the Fabrication of Membrane-Based NEMS Devices", *Microelectron. Eng.*, 159, 108– 113, 2016.

[6] C. –K. Lee, Y. Hwangbo, S. –M. Kim, S. –K. Lee, S. –M. Lee, S. –S. Kim, K. –S. Kim, H. –J. Lee, B. –I. Choi, C. –K. Song, J. –H. Ahn and J. –H. Kim, "Monatomic Chemical-Vapor-Deposited Graphene Membranes Bridge a Half-Millimeter-Scale Gap", *ACS Nano*, 8, 2336– 2344, 2014.

[7] S. A. Akbari, V. Ghafarinia, T. Larsen, M. M. Parmar and L. G. Villanueva, "Large Suspended Monolayer and Bilayer Graphene Membranes with Diameter up to 750 µm", *Sci. Rep.*, 10, 6426, 2016.

[8] Y. –M. Chen, S. –M. He, C. –H. Huang, C. –C. Huang, W. –P. Shih, C. –L. Chu, J. Kong, J. Li and C. –Y. Su, "Ultra-large Suspended Graphene as a Highly Elastic Membrane for Capacitive Pressure Sensors", *Nanoscale*, 8, 3555– 3564, 2016.

[9] A. F. Carvalho, A. J. Fernandes, M. B. Hassine, P. Ferreira, E. Fortunato and F. M. Costa, "Millimeter-Sized Few-Layer Suspended Graphene Membranes", *Applied Materials Today*, 21, 100879, 2020.

[10] J. Xu, G. S. Wood, E. Mastropaolo, M. J. Newton and R. Cheung, "Realization of a Graphene/PMMA Acoustic Capacitive Sensor Released by Silicon Dioxide Sacrificial Layer", *ACS Appl. Mater. Interfaces*, 13, 38792– 38798, 2021.

[11] G. Baglioni, R. Pezone, S. Vollebregt, K. C. Zobenića, M. Spasenović, D. Todorović, H. Liu, G. Verbiest, H. S. van der Zant and P. G. Steeneken, "Optical Characterization of Ultra Sensitive Graphene Membranes for Microphone Applications", *Under review, 2022*.

[12] A. Shchepetov, M. Prunnila, F. Alzina, L. Schneider, J. Cuffe, H. Jiang, E. I. Kauppinen, C. M. S. Torres and J. Ahopelto, "Ultra-Thin Free-Standing Single Crystalline Silicon Membranes with Strain Control", *Appl. Phys. Lett.*, 102, 192108, 2013.

[13] F. Ricciardella, S. Vollebregt, T. Polichetti, M. Miscuglio, B. Alfano, M. L. Miglietta, E. Massera, G. Di Francia and P. M. Sarro, "Effects of Graphene Defects on Gas Sensing Properties towards NO2 Detection", *Nanoscale,* 9, 6085– 6093, 2017.

[14] L. Malard, M. Pimenta, G. Dresselhaus, and M. Dresselhaus, "Raman Spectroscopy in Graphene", *Phys. Rep*, 473, 51 - 87, 2009.

[15] R. Pezone, G. Baglioni, P. M. Sarro, P. G. Steeneken and S. Vollebregt, "Sensitive Transfer-Free Wafer-Scale Graphene Microphones", *ACS Appl. Mater. Interfaces*, 14 (18), 21705-21712, 2022.=

CONTACT

*R. Pezone, public mail: r.pezone@tudelft.com